Journal of Computational Physics 486 (2023) 112128

Contents lists available at ScienceDirect

Journal of Computational Physics

journal homepage: www.elsevier.com/locate/jcp

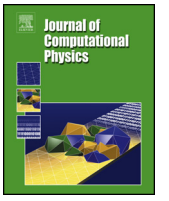

A time-relaxed Monte Carlo method preserving the Navier-Stokes asymptotics

Fei Fei

School of Aerospace Engineering, Huazhong University of Science and Technology, 430074 Wuhan, China

ARTICLE INFO

Article history:
Received 1 November 2022
Received in revised form 9 March 2023
Accepted 3 April 2023
Available online 6 April 2023

Keywords:
Boltzmann equation
Monte Carlo method
Asymptotic preserving scheme
Multiscale flows

ABSTRACT

In this paper, a new time-relaxed Monte Carlo (TRMC) method is proposed for the inhomogeneous Boltzmann equation. Compared to the standard TRMC scheme, the proposed method performs the same convection operator, however, divides the collision operator by a micro-macro decomposition. The continuous part of the collision operator is constructed based on the first-order Chapman-Enskog expansion and solved by an explicit second-order scheme, while the numerical solution of the rest nonequilibrium part is still provided by the standard TRMC scheme. In this way, the new TRMC method demonstrates the same accuracy as the standard TRMC scheme in the kinetic limit, however, preserves Navier-Stokes asymptotics and the second-order accuracy in the fluid limit. Several numerical cases of inhomogeneous flows, such as the one-dimensional Poiseuille flow, Sod tube flow, the shock wave and two-dimensional hypersonic flow past a cylinder, are calculated and compared with direct simulation Monte Carlo (DSMC) or Navier-Stokes solutions. It is noted that the new TRMC scheme is more accurate and efficient than the standard TRMC and DSMC methods for simulations of multi-scale gas flows.

1. Introduction

Multi-scale gas flows, which include both continuum and rarefied flow regimes, widely exist in aerospace and micro-electro-mechanical systems. Different flow regimes are identified by the Knudsen (Kn) number, which is the ratio between the mean free path of the molecules and the characteristic length of the flow field. In a continuum flow regime, a gas flow near the equilibrium state can be simulated by a gas dynamic scheme, such as computational fluid dynamic (CFD) based on Euler or Navier-Stokes equations. Conversely, in a rarefied flow regime, a gas flow departs far from thermodynamical equilibrium, and a kinetic approach, which tracks molecular motions and collisions individually, is necessary. However, if the Kn number varies over several orders of magnitude in the flow field, neither the dynamic nor the kinetic treatment is appropriate. A pure gas dynamic method will lose physics where the Kn number is large, while a standard kinetic scheme, such as the direct simulation Monte Carlo (DSMC) method [1], is very expansive with a small Kn number due to the numerical stiffness. To reach a compromise between computational accuracy and efficiency, domain decomposition methods, such as the hybrid CFD-DSMC algorithms [2–5], were established. It divides the computational domain into a continuous region, which is solved by a CFD scheme, and a rarefied region, which is calculated by a kinetic one. The key point of this hybrid CFD-DSMC method is how to decompose the computational domain. However, finding a common

E-mail address: ffei@hust.edu.cn.

https://doi.org/10.1016/j.jcp.2023.112128
0021-9991/

continuum-breakdown criterion to position the interface between the continuous and rarefied regions is not easy [6–8]. Therefore, besides the hybrid CFD-DSMC method, several particle-particle hybrid schemes are also proposed recently, such as the BGK-DSMC [10], FP-DSMC [11] and USPBGK-DSMC [12] methods. They employ a stochastic particle method based on the Bhatnagar-Gross-Krook (BGK) or Fokker-Planck model to simulate the continuous region. Since kinetic models can be applied to a much wider range of the Kn number, the choice of the breakdown criterion is more flexible compared to the hybrid CFD-DSMC method [9]. However, extending these particle-particle hybrid schemes for complex gases, such as including multi-species or chemical reactions, is still problematic due to the lack of accurate kinetic models.

In addition to the idea of domain decomposition, another strategy, direct starting from a kinetic scheme, is to design a suitable time discretization of the Boltzmann equation for a wide range of Kn numbers. In consideration of Monte Carlo methods, this class of algorithms includes the time relaxed [13,14], exponential Runge–Kutta [15] and asymptotic-preserving Monte Carlo methods [16]. The main interest is that their time steps are not constrained by the mean collision time. Therefore, these multiscale Monte Carlo methods are much more efficient than the conventional DSMC method. In detail, if the time step is fixed, for a large Kn number, they are consistent with a standard kinetic scheme of the Boltzmann equation; and when the Kn number decreases, their numerical solutions tend to a local Maxwellian. This is the well-known property called asymptotic preservation (AP) [17] and a related algorithm is the AP scheme. To our knowledge, most of the existing Monte Carlo methods with AP property only preserve the Euler asymptotics. Therefore, they are struggling to accurately capture shear stress and heat flux in the fluid limit [16]. However, the viscous effect is important in several circumstances, such as the boundary layer and vortex flows. An exception is the Monte Carlo method [20] based on the micro-macro decomposition [18,19]. Since the micro-macro decomposition scheme treats a perturbation probability distribution function (PDF) deviated from the Maxwellian, an AP property of Navier-Stokes equations can be obtained. But the perturbation PDF will also introduce particles with negative weights, which are quite complicated to deal with in the collision process of DSMC [20].

The goal of this work is to develop a new asymptotic-preserving Monte Carlo method preserving the Navier-Stokes asymptotics and second-order accuracy. Starting from the standard time-relaxed Monte Carlo (TRMC) method [14,21], the collision operator of the proposed scheme is also derived from the Wild sum expansion of the homogeneous Boltzmann equation [22]. However, unlike a Maxwellian truncation in the standard TRMC method, a micro-macro decomposition to the collision operator, which is based on the Chapman-Enskog expansion [23,24], is employed to achieve an AP property of NS equations. Generally speaking, the proposed TRMC method is constructed by directly combining the DSMC and a continuous model, such as the Navier-Stokes solution in the present work. Therefore, it is independent of the special kinetic model in contrast to the existing particle-particle hybrid schemes.

The rest of the paper is organized as follows. In Section 2, we briefly review the DSMC and TRMC methods. After that, a new asymptotic-preserving Monte Carlo method, which is based on the standard TRMC method and preserves the Navier-Stokes asymptotics, is developed and analyzed in Section 3. In Section 4, the proposed method is validated by several inhomogeneous problems in various flow regimes. The numerical results show that the proposed method can achieve a higher order of accuracy and perform better than the standard TRMC and DSMC methods in the simulation of multiscale flows. The paper is concluded in Section 5.

2. Review of the time-relaxed Monte Carlo method

2.1. The Boltzmann equation

From the viewpoint of kinetic theory, a gas flow is governed by the Boltzmann equation, i.e.,

$$\frac{\partial f(\mathbf{V};\mathbf{x},t)}{\partial t} + V_i \frac{\partial f(\mathbf{V};\mathbf{x},t)}{\partial x_i} = \frac{1}{\varepsilon} Q(f,f), \tag{2.1}$$

where $f(\mathbf{V};\mathbf{x},t)$ is the probability density function (PDF) of gas molecules with velocity $\mathbf{V}$ at position $\mathbf{x}$ and time t. For simplicity, monoatomic gas is considered in the present work. The right-hand side of Eq. (2.1) refers to the Boltzmann collision term, in which $Q(f,f)$ describes the binary collisions of molecules and is given as

$$Q(f,f) = \int_{\mathbb{R}^3}\int_{\mathbb{S}^2} \left[f(\mathbf{V}')f(\mathbf{V}_1') - f(\mathbf{V})f(\mathbf{V}_1)\right] c_r \sigma d\Omega d\mathbf{V}_1, \tag{2.2}$$

where $\mathbf{V}$ and $\mathbf{V}_1$ are pre-collisional velocities of collision pair and $\mathbf{V}'$ and $\mathbf{V}_1'$ represent their post-collisional velocities. $c_r = |\mathbf{V} - \mathbf{V}_1|$ is the relative velocity of the colliding molecules. σ is the differential cross-section of the binary collision. Ω is the solid angle. Here, Eq. (2.1) is written in a dimensionless form and the parameter ε is related to the Kn number.

The Boltzmann collision term preserves mass, momentum and energy, i.e.,

$$\int_{\mathbb{R}^3} Q(f,f)\phi(\mathbf{V})d\mathbf{V} = 0, \quad \phi(\mathbf{V}) = 1, \mathbf{V}, V^2. \tag{2.3}$$

Therefore, taking the ensemble average of Eq. (2.1) with $\phi(\mathbf{V})$, the conservation equations are obtained as

$$\frac{\partial \rho}{\partial t} + \frac{\partial (\rho u_i)}{\partial x_i} = 0, \tag{2.4a}$$

$$\frac{\partial (\rho u_i)}{\partial t} + \frac{\partial \left(\rho u_i u_j\right)}{\partial x_j} + \frac{\partial P_{ij}}{\partial x_j} = 0, \tag{2.4b}$$

$$\frac{\partial (\rho e)}{\partial t} + \frac{\partial (\rho u_i e)}{\partial x_i} + P_{ij}\frac{\partial u_j}{\partial x_i} + \frac{\partial q_i}{\partial x_i} = 0, \tag{2.4c}$$

where ρ is the density; $\mathbf{u}$ is the macroscopic velocity; $e = 3RT/2$ is the internal energy, T is the temperature and R is the gas constant.

$$P_{ij} = \int_{\mathbb{R}^3} C_i C_j f d\mathbf{V} \quad \text{and} \quad q_i = \int_{\mathbb{R}^3} \frac{1}{2} C_i C^2 f d\mathbf{V} \tag{2.5}$$

are the pressure tensor and heat flux, respectively. $\mathbf{C} = \mathbf{V} - \mathbf{u}$ denotes the peculiar velocity of molecules. In general, since the pressure tensor and heat flux are dependent on the details of the PDF, the conservation equations are not closed. However, the Euler and Navier-Stokes (NS) equations can be obtained from the Chapman-Enskog theory. Using Chapman-Enskog expansion [36], the PDF can be written as a series corresponding to the Kn number, i.e.,

$$f = f^{(0)} + f^{(1)} + f^{(2)} + \cdots, \tag{2.6}$$

where $f^{(0)} = f_M$ is the Maxwellian distribution,

$$f_M = \rho \left(\frac{1}{2\pi T}\right)^{3/2} \exp\left(-\frac{C^2}{2T}\right). \tag{2.7}$$

$f^{(1)}$ and $f^{(2)}$ refer to the first and second-order Chapman-Enskog expansions, and $f^{(1)}$ is given as

$$f^{(1)} = f_M \left[\frac{1}{2pT}\left(\mathbf{C} \otimes \mathbf{C} - \frac{1}{3}C^2\mathbf{I}\right) : \boldsymbol{\sigma}^{(1)} + \frac{2}{5}\frac{1}{pT}\mathbf{C} \cdot \mathbf{q}^{(1)}\left(\frac{C^2}{2T} - \frac{5}{2}\right)\right], \tag{2.8}$$

where p is the pressure.

$$\boldsymbol{\sigma}^{(1)} = -\frac{1}{\mathrm{Re}}\left(\nabla \mathbf{u} + (\nabla \mathbf{u})^T - \frac{2}{3}\nabla \cdot \mathbf{u} I\right) \quad \text{and} \quad \mathbf{q}^{(1)} = -\frac{5}{2}\frac{\mathrm{Pr}}{\mathrm{Re}}\nabla T \tag{2.9}$$

are the first-order expansion of stress and heat flux, respectively. Pr is the Prandtl number and the Reynolds number is defined as $\mathrm{Re} = \left(\rho^* x^* \sqrt{RT^*}\right)/\mu$. x^*, ρ^* and T^* are characteristic length, density and temperature, respectively. μ refers to the gas viscosity.

In the equilibrium state $f = f_M$, $P_{ij} = \rho RT\delta_{ij}$ and $q_i = 0$, then Eq. (2.4) reduces to the Euler equations. Here δ_{ij} is the Kronecker delta function. Otherwise, if the PDF is assumed as the first-order of Chapman-Enskog expansion, i.e., $f = f_M + f^{(1)}$, Navier-Stokes equations can be obtained from Eq. (2.4).

2.2. The DSMC method

As the Knudsen number increases, the gas flow departs far away from equilibrium and the Navier-Stokes equations become inappropriate. Therefore, in the rarefied flow regime, the Boltzmann equation should be calculated instead. To solve the Boltzmann equation, one can either represent PDF using discrete velocity points or stochastic particles [25]. Because of the high dimensionality of the Boltzmann equation, the former one is usually computationally expensive, especially for hypersonic gas flows. In contrast, the memory consumption of the stochastic particle method is much smaller, which is only dependent on the particle number. The most prominent stochastic particle algorithm is the direct simulation Monte Carlo (DSMC) method [1]. Using a simple operator splitting scheme, DSMC calculates the particle convection and collision processes successively, as it were, the Boltzmann equation (2.1) is solved with two steps:

$$\text{Convection:} \quad \frac{\partial f}{\partial t} + V_i \frac{\partial f}{\partial x_i} = 0 \quad \text{and} \tag{2.10a}$$

$$\text{Collision:} \quad \frac{\partial f}{\partial t} = \frac{1}{\varepsilon} Q\left(f, f\right). \tag{2.10b}$$

During the convection step, particles' velocities are unchanged and their positions are updated like in free molecular motion. Therefore, the numerical solution of PDF is evolved as

$$f^*(\mathbf{V}; \mathbf{x}) = \mathcal{T}_{\Delta t}(f^n) = f^n(\mathbf{V}; \mathbf{x} - \mathbf{V}\Delta t). \tag{2.11}$$

$f^n(\mathbf{V};\mathbf{x})$ denotes the initial PDF at time $n\Delta t$, Δt is the time step; $f^*(\mathbf{V};\mathbf{x})$ refers to the PDF solution after the convection step. $\mathcal{T}_{\Delta t}(f)$ is defined as the convection operator.

During the collision step, particles' positions keep constant while their velocities are calculated based on the dynamics of binary collisions. To reproduce the actual mean collision rate, collision pairs should be carefully selected. Bird's no time counter (NTC) scheme [1] and Nanbu-Babovsky's scheme [26] are the most used two sampling algorithms. For example, in the framework of Nanbu-Babovsky's scheme, the governing equation of the collision step, i.e., Eq. (2.10b), is rewritten as

$$\frac{\partial f}{\partial t} = \frac{1}{\varepsilon}\left[P(f,f) - \beta f\right]. \tag{2.12}$$

If Maxwellian molecules are employed, we can set $P(f,f) = Q^+(f,f)$ and $\beta = Q^-(f)$, therefore $Q^+(f,f)$ and $Q^-(f)$ are given as

$$Q^+(f,f) = \int_{\mathbb{R}^3}\int_{\mathbb{S}^2} f(\mathbf{V}')f(\mathbf{V}_1')c_r\sigma d\Omega d\mathbf{V}_1 \quad \text{and} \tag{2.13a}$$

$$Q^-(f) = \int_{\mathbb{R}^3}\int_{\mathbb{S}^2} f(\mathbf{V}_1)c_r\sigma d\Omega d\mathbf{V}_1, \tag{2.13b}$$

which denote the gain and loss terms of the Boltzmann collision term, respectively. Considering $f^*(\mathbf{V};\mathbf{x})$ as the initial condition and solving Eq. (2.12) using the forward Euler scheme, we have

$$f^{n+1}(\mathbf{V};\mathbf{x}) = \mathcal{C}_{\Delta t}^{DSMC}(f^*) = \left(1 - \frac{\beta\Delta t}{\varepsilon}\right)f^* + \frac{\beta\Delta t}{\varepsilon}\frac{P(f^*,f^*)}{\beta}, \tag{2.14}$$

where $\mathcal{C}_{\Delta t}^{DSMC}(f)$ is defined as the collision operator of DSMC. The probabilistic interpretation of Eq. (2.14) is that, in DSMC simulation a particle will not collide with probability $(1-\beta\Delta t/\varepsilon)$, and collide following the collision operator $P(f^*,f^*)$ with probability $\beta\Delta t/\varepsilon$. From Eq. (2.14), it is also observed that the time step of DSMC is restricted by ε/β. Otherwise, too large time step will lead the coefficient of the first term of Eq. (2.14) negative and the assumption of the decoupling of particle motion and collision invalid. Therefore, if applied to the continuum flow regime, i.e., $\varepsilon \to 0$, the conventional DSMC method will show strong numerical stiffness and become quite inefficient. To overcome this defect, several Monte Carlo methods with the asymptotic preserving (AP) property have been proposed, such as the time-relaxed Monte Carlo (TRMC) method [14]. The AP property allows the TRMC method to recover the Euler solution as $\varepsilon \to 0$.

2.3. The TRMC method

2.3.1. The numerical scheme of TRMC

Starting from the homogeneous Boltzmann equation, the TRMC method replaces the time variable t and PDF f with the expressions

$$t' = 1 - e^{-\beta t/\varepsilon} \quad \text{and} \quad F(\mathbf{V};\mathbf{x},t') = f(\mathbf{V};\mathbf{x},t)e^{\beta t/\varepsilon}. \tag{2.15}$$

Then, Eq. (2.12) is rewritten as

$$\frac{\partial F}{\partial t'} = \frac{1}{\beta}P(F,F). \tag{2.16}$$

Its numerical solution after the time step Δt is constructed using the first $m+1$ terms of Wild Sum [22], and given as

$$f^{n+1} = \mathcal{C}_{\Delta t}^{TRMC}(f^*) = \sum_{k=0}^{m} A_k f_k + A_{m+1} f_M. \tag{2.17}$$

Similarly, $\mathcal{C}_{\Delta t}^{TRMC}(f)$ is defined as the collision operator of TRMC, and m denotes the order of the TRMC method. The functions f_k are given by the recurrence formula

$$f_{k+1}(\mathbf{V}) = \frac{1}{k+1}\sum_{h=0}^{k}\frac{1}{\beta}P\left(f_h, f_{k-h}\right), \quad k = 0,1,.... \quad \text{and} \tag{2.18a}$$

$$f_0(\mathbf{V}) = f^*(\mathbf{V};\mathbf{x}). \tag{2.18b}$$

A_k are nonnegative weight functions. In the standard TRMC method [14], a choice of these functions is given by

$$A_k = e^{-\beta\Delta t/\varepsilon}\left(1 - e^{-\beta\Delta t/\varepsilon}\right)^k, k = 0,\ldots,m-1, \quad A_m = 1 - \sum_{k=0}^{m-1}A_k - A_{m+1}, \quad A_{m+1} = \left(1 - e^{-\beta\Delta t/\varepsilon}\right)^{m+2}. \tag{2.19}$$

However, other choices of these parameters are also possible [27]. The probabilistic interpretation of Eq. (2.17) is that simulated particles are unchanged with probability A_0, performed multiple collision processes with probability A_k ($k \in [1, m]$), and sampled from the Maxwellian distribution with probability A_{m+1}. In addition, Gabetta et al. [13] have proved that for any $m \geq 1$, $\lim_{\beta\Delta t/\varepsilon \to \infty} f^{n+1} = f_M$, therefore, the standard TRMC method satisfied the AP property of Euler equations.

Besides Maxwellian molecules, the TRMC method can also be applied to other molecule models. Pareschi and Russo [14] have given a general expression of $P(f, f)$, i.e.,

$$P(f, f) = Q(f, f) + \beta f = Q^+(f, f) + f\left(\beta - Q^-(f)\right), \tag{2.20}$$

and the constant β should satisfy

$$\beta \geq Q^-(f). \tag{2.21}$$

The details of the TRMC method with the variable hard sphere (VHS) molecules are referred to the reference [14].

2.3.2. The accuracy of the TRMC method

In the kinetic limit ($\beta\Delta t/\varepsilon \ll 1$), Gabetta et.al. [13] have shown that the time relaxed scheme can obtain m^{th} order of accuracy with numerical solution (2.17) for the homogeneous Boltzmann equation. However, in practice, the accuracy of the TRMC method will also be influenced by the choice of β [28].

For the inhomogeneous Boltzmann equation, the simple splitting scheme as DSMC is usually employed in TRMC, i.e., $f^{n+1} = \mathcal{C}_{\Delta t}^{TRMC}\left[\mathcal{T}_{\Delta t}\left(f^n\right)\right]$. The simple splitting scheme only has first order accuracy even though we solve both particle motion and collision steps with great accuracy. To improve the accuracy in time, another choice is the Strang splitting scheme [29], i.e.,

$$f^{n+1} = \mathcal{T}_{\Delta t/2}\left\{\mathcal{C}_{\Delta t}^{TRMC}\left[\mathcal{T}_{\Delta t/2}\left(f^n\right)\right]\right\}. \tag{2.22}$$

Using the Strang splitting scheme, TRMC can achieve second order of accuracy in the kinetic limit, if both the convection and collision steps are at least second order.

In the fluid limit ($\beta\Delta t/\varepsilon \gg 1$), however, the Strang splitting scheme of the standard TRMC method cannot preserve accuracy. We demonstrate it in the following. As $\beta\Delta t/\varepsilon \gg 1$, the numerical solution of the TRMC collision operator approaches the equilibrium state as shown in Eq. (2.17). Therefore, according to Eq. (2.22), at the half time step its PDF solution can be assumed as Maxwellian $f_M^{n+1/2}$. Correspondingly, macroscopic variables are calculated as $U^{n+1/2} = \left\langle \phi(\mathbf{V}) f_M^{n+1/2} \right\rangle$, where $\langle \cdots \rangle$ denotes the ensemble average. In addition, according to the Strang splitting scheme as shown in Eq. (2.22), $f_M^{n+1/2}$ is calculated from the convection of the PDF at time $(n-1/2)\Delta t$; thus, the numerical solution of $U^{n+1/2}$ is also written as

$$U_{TRMC}^{n+1/2} = \left\langle \phi(\mathbf{V}) f_M^{n-1/2}(\mathbf{V}; \mathbf{x} - \mathbf{V}\Delta t) \right\rangle. \tag{2.23}$$

Then, taking Taylor expansion at time $(n-1/2)\Delta t$ and position $\mathbf{x}$, Eq. (2.23) can be rewritten as

$$\begin{aligned} U_{TRMC}^{n+1/2} = &\left\langle \phi(\mathbf{V}) f_M^{n-1/2}(\mathbf{V}; \mathbf{x}) \right\rangle - \Delta t \frac{\partial}{\partial x}\left\langle \mathbf{V}\phi(\mathbf{V}) f_M^{n-1/2}(\mathbf{V}; \mathbf{x}) \right\rangle \\ &+ \frac{1}{2}\Delta t^2 \frac{\partial^2}{\partial x^2}\left\langle \mathbf{V}^2\phi(\mathbf{V}) f_M^{n-1/2}(\mathbf{V}; \mathbf{x}) \right\rangle + O(\Delta t^3). \end{aligned} \tag{2.24}$$

Conversely, from the viewpoint of gas dynamics, macroscopic variables also satisfy Euler equations in the equilibrium state, i.e.,

$$\frac{\partial U}{\partial t} = \mathcal{T}(U), \quad \text{and} \tag{2.25}$$

$$\mathcal{T}(U) = -\frac{\partial}{\partial x}\left\langle \mathbf{V} f_M(\mathbf{V}; x, t)\phi(\mathbf{V}) \right\rangle. \tag{2.26}$$

Based on Eqs. (2.25) and (2.26), Taylor expansion of the solution $U^{n+1/2}$ at time step $(n-1/2)\Delta t$ and position $\mathbf{x}$ can be calculated as

$$U^{n+1/2} = U^{n-1/2} + \Delta t\mathcal{T}(U^{n-1/2}) + \frac{\Delta t^2}{2}\frac{\partial \mathcal{T}(U^{n-1/2})}{\partial t} + O(\Delta t^3), \quad \text{and} \tag{2.27}$$

$$\frac{\partial \mathcal{T}(U^{n-1/2})}{\partial t} = -\frac{\partial}{\partial x}\left\langle \mathbf{V}\frac{\partial f_M^{n-1/2}(\mathbf{V}; x)}{\partial U}\phi(\mathbf{V})\mathcal{T}(U^{n-1/2}) \right\rangle. \tag{2.28}$$

Comparing Eqs. (2.24) and (2.27), their difference is obtained as

$$U_{TRMC}^{n+1/2} - U^{n+1/2} = \frac{1}{2}\Delta t^2 \frac{\partial}{\partial x}\left\langle \mathbf{V}\frac{\partial f_M^{n-1/2}(\mathbf{V};\mathbf{x})}{\partial U}\phi(\mathbf{V})\frac{\partial(\mathbf{V}U^{n-1/2})}{\partial x}\right\rangle + \frac{1}{2}\Delta t^2 \frac{\partial}{\partial x}\left\langle \mathbf{V}\frac{\partial f_M^{n-1/2}(\mathbf{V};x)}{\partial U}\phi(\mathbf{V})\mathcal{T}(U^{n-1/2})\right\rangle + O(\Delta t^3). \tag{2.29}$$

Since $\mathbf{V}U^{n-1/2} = \mathbf{V}\left\langle f_M^{n-1/2}(\mathbf{V};x)\,\phi(\mathbf{V})\right\rangle \neq \left\langle \mathbf{V} f_M^{n-1/2}(\mathbf{V};x,t)\,\phi(\mathbf{V})\right\rangle$ in general [30], therefore,

$$U_{TRMC}^{n+1/2} = U^{n+1/2} + O(\Delta t^2). \tag{2.30}$$

It indicates that the Strang splitting scheme of the standard TRMC method is only first order accurate in the fluid limit. This order reduction of the Strang splitting scheme has also been discussed by Jin [31] for hyperbolic systems with stiff relaxation terms.

3. A TRMC method preserving the Navier-Stokes asymptotics

As discussed in Section 2, the existing TRMC method preserves the Euler asymptotics and only has first order of accuracy in the fluid limit. To improve its performance in the continuum flow regime, a new TRMC method is proposed in this work. To summarize, the main features of this proposed scheme would be:

- Asymptotic preserving property of NS equations;
- Asymptotic preserving second-order accurate in the fluid limit and the same order accurate as the standard TRMC method in the kinetic limit;
- Implemented with stochastic particles like DSMC.

In addition, we call this proposed method as the AAP-TRMC (asymptotic accurate and preserving TRMC) method for short in the present work.

3.1. The numerical scheme

In the proposed TRMC method, to reach a high order accuracy for the inhomogeneous Boltzmann equation, the Strang splitting scheme as shown in Eq. (2.22) is also employed, therefore, its numerical solution during a time step can be written as

$$f^{n+1} = \mathcal{T}_{\Delta t/2}\left\{\mathcal{C}_{\Delta t}^{AAP-TRMC}\left[\mathcal{T}_{\Delta t/2}\left(f^n\right)\right]\right\}. \tag{3.1}$$

The convection operator is as same as that of the standard TRMC scheme, however, its collision operator $\mathcal{C}_{\Delta t}^{AAP-TRMC}$ is constructed based a micro-macro decomposition [23,24] as followers:

First, using the Chapman-Enskog expansion (2.6), the Boltzmann collision term can also be expanded as

$$Q(f,f) = Q^{(0)}(f) + Q^{(1)}(f) + Q^{(2)}(f) + \cdots, \tag{3.2}$$

where $Q^{(0)}(f) = 0$; $Q^{(1)}(f) = 2Q\left(f^{(0)}, f^{(1)}\right)$ and $Q^{(2)}(f)$ represent the first and second order expansions, respectively. Note that $Q^{(1)}$ is a linear operator. Therefore, the first order expansion of the standard TRMC collision operator, i.e., Eq. (2.17), can be written as

$$\mathcal{C}_{\Delta t}^{TRMC,(1)}(f^*) = \sum_{k=0}^{m} A_k f_k^{(1)}. \tag{3.3}$$

According to Eq. (2.18),

$$f_{k+1}^{(1)}(\mathbf{V}) = \frac{1}{k+1}\sum_{h=0}^{k}\frac{1}{\beta}P^{(1)}\left(f_h, f_{k-h}\right), \quad k = 0, 1, \ldots. \quad \text{and} \tag{3.4a}$$

$$f_0^{(1)}(\mathbf{V}) = f^{*,(1)}(\mathbf{V};\mathbf{x}), \tag{3.4b}$$

where $f^*(\mathbf{V};\mathbf{x}) = \mathcal{T}_{\Delta t/2}\left(f^n\right)$ denotes the numerical solution after particle convection for half time step, and $P^{(1)}(f,f) = Q^{(1)}(f) + \beta f^{(1)}$.

Second, we keep the high order expansions of the standard TRMC collision operator unchanged, however, replace the first order one, i.e., Eq. (3.3), by the numerical solution of a second order scheme, which is

$$\mathcal{C}_{\Delta t}^{AAP-TRMC,(1)}\left(f^*\right) = f^{*,(1)} + \frac{\Delta t}{\varepsilon}Q^{(1)}\left(f^*\right) + \frac{1}{2}\left(\frac{\Delta t}{\varepsilon}\right)^2 Q^{(1)}\left(Q^{(1)}\left(f^*\right)\right). \tag{3.5}$$

It is noted that $\partial\left[Q^{(1)}(f^*)\right]/\partial t = Q^{(1)}\left(Q^{(1)}(f^*)\right)$ as $Q^{(1)}$ is a linear operator. Therefore, combining Eqs. (2.17), (3.3) and (3.5), the collision operator of the proposed method is reconstructed as

$$\begin{aligned}\mathcal{C}_{\Delta t}^{AAP-TRMC}(f^*) &= \mathcal{C}_{\Delta t}^{TRMC}(f^*) - \mathcal{C}_{\Delta t}^{TRMC,(1)}(f^*) + \mathcal{C}_{\Delta t}^{AAP-TRMC,(1)}\left(f^*\right) \\ &= \sum_{k=0}^{m} A_k f_k + A_{m+1}\left(f_M^{n+1/2} + f_\alpha\right),\end{aligned} \tag{3.6}$$

where $f_\alpha = \frac{1}{A_{m+1}}\left\{f^{*,(1)} + \frac{\Delta t}{\varepsilon}Q^{(1)}(f^*) + \frac{1}{2}\left(\frac{\Delta t}{\varepsilon}\right)^2 Q^{(1)}\left[Q^{(1)}(f^*)\right] - \sum_{k=0}^{m} A_k f_k^{(1)}\right\}$, and $f_M^{n+1/2}$ is defined as the Maxwellian corresponding to f^*. Compared to the standard TRMC method, an additional PDF f_α is introduced in the last term of right-hand side of Eq. (3.6).

Third, according to the convection operator, we assume that f^* is approximated as

$$f^{*,(1)}(\mathbf{V};\mathbf{x}) \approx f_M^{n+1/2} + f^{n+1/2,(1)} - \frac{\Delta t}{2\varepsilon}Q^{(1)}\left(f^{n+1/2}\right), \tag{3.7}$$

and

$$f^{n+1/2,(1)} = f_M^{n+1/2}\left[\frac{1}{2pT}\left(\mathbf{C}\otimes\mathbf{C} - \frac{1}{3}C^2\mathbf{I}\right):\boldsymbol{\sigma}^{(1)} + \frac{2}{5}\frac{1}{pT}\mathbf{C}\cdot\mathbf{q}^{(1)}\left(\frac{C^2}{2T} - \frac{5}{2}\right)\right] \quad \text{and} \tag{3.8a}$$

$$\begin{aligned}Q^{(1)}\left(f^{n+1/2}\right) &= \varepsilon\left(\frac{\partial_0 f_M^{n+1/2}}{\partial t} + V_i\frac{\partial f_M^{n+1/2}}{\partial x_i}\right) \\ &= -\frac{f_M^{n+1/2}}{\mu/(p\varepsilon)}\left[\frac{1}{2pT}\left(\mathbf{C}\otimes\mathbf{C} - \frac{1}{3}C^2\mathbf{I}\right):\boldsymbol{\sigma}^{(1)} + \frac{2}{5}\frac{1}{pT}\Pr\mathbf{C}\cdot\mathbf{q}^{(1)}\left(\frac{C^2}{2T} - \frac{5}{2}\right)\right].\end{aligned} \tag{3.8b}$$

$\boldsymbol{\sigma}^{(1)}$ and $\mathbf{q}^{(1)}$, which represent the first order expansion of stress and heat flux, are given by Eq. (2.9). Then, using the approximations of $f^{*,(1)}$, f_α can be derived as

$$f_\alpha = \frac{1}{A_{m+1}}f_M^{n+1/2}\left\{\begin{array}{l}\left[1 - \dfrac{\Delta t}{2\mu/p} - \left(1 + \dfrac{\Delta t}{2\mu/p}\right)\Phi_1\right]\dfrac{1}{2pT}\left(\mathbf{C}\otimes\mathbf{C} - \dfrac{1}{3}C^2\mathbf{I}\right):\boldsymbol{\sigma}^{(1)} \\ +\left[1 - \dfrac{\Delta t}{2\mu/p}\Pr - \left(1 + \dfrac{\Delta t}{2\mu/p}\Pr\right)\Phi_2\right]\dfrac{2}{5}\dfrac{1}{pT}\mathbf{C}\cdot\mathbf{q}^{(1)}\left(\dfrac{C^2}{2T} - \dfrac{5}{2}\right)\end{array}\right\}, \tag{3.9}$$

where higher order terms, such as $O(\Delta t)^3$, are omitted. Φ_1 and Φ_2 are coefficient functions dependent on the time step size and distinct for the TRMC method with different orders. In detail, the collision operator for first order AAP-TRMC method (AAP-TRMC1) is written as

$$\mathcal{C}_{\Delta t}^{AAP-TRMC1}\left(f^*\right) = A_0 f^* + A_1\frac{P(f^*,f^*)}{\beta} + A_2\left(f_M^{n+1/2} + f_\alpha\right), \tag{3.10}$$

and

$$\Phi_1 = A_0 + A_1\left(1 - \chi^{-1}\right) \text{ and } \Phi_2 = A_0 + A_1\left(1 - \Pr\chi^{-1}\right), \tag{3.11}$$

where $\chi = \mu\beta/(p\varepsilon)$. For the second order AAP-TRMC method (AAP-TRMC2), the collision operator is given as

$$\mathcal{C}_{\Delta t}^{AAP-TRMC2}\left(f^*\right) = A_0 f^* + A_1\frac{P(f^*,f^*)}{\beta} + A_2\frac{P(f^*,f_1)}{\beta} + A_3\left(f_M^{n+1/2} + f_\alpha\right), \tag{3.12}$$

and

$$\Phi_1 = A_0 + \left(A_1 + \frac{1}{2}A_2\right)\left(1 - \chi^{-1}\right) + \frac{1}{2}A_2\left(1 - \chi^{-1}\right)^2 \quad \text{and} \tag{3.13a}$$

$$\Phi_2 = A_0 + \left(A_1 + \frac{1}{2}A_2\right)\left(1 - \Pr\chi^{-1}\right) + \frac{1}{2}A_2\left(1 - \Pr\chi^{-1}\right)^2. \tag{3.13b}$$

3.2. Properties of the AAP-TRMC method

3.2.1. Positivity

Following the Strang splitting scheme, the AAP-TRMC method calculates the particle convection and collision operators separately. As a stochastic particle method, the particle convection operator is positivity preserving in any time. For the collision operator, the coefficients A_k of the AAP-TRMC method are as same as those from the standard TRMC method,

which always keep positive [14]. However, it should be mentioned that in the AAP-TRMC collision operator, the velocities of computational particles, which belong to the last term of Eq. (3.6), are resampled from the PDF $\left(f_M^{n+1/2}+f_\alpha\right)$. Since f_α is constructed based on the Chapman-Enskog expansion as shown in Eq. (3.9), the PDF $\left(f_M^{n+1/2}+f_\alpha\right)$ may include negative part as the Kn number increases. To avoid this situation, we introduce a scaling factor θ before f_α to ensure the positivity in the simulation, as it were, $\left(f_M^{n+1/2}+f_\alpha\right)$ is replaced by $\left(f_M^{n+1/2}+\theta f_\alpha\right)$ and

$$\theta=\begin{cases}1 & \beta\Delta t/\varepsilon\geq 1\\ \min\left\{1,\dfrac{\varepsilon}{\beta\Delta t}A_{m+1}\right\} & \beta\Delta t/\varepsilon<1\end{cases}. \tag{3.14}$$

In the fluid limit, as $\beta\Delta t/\varepsilon\gg 1$, $A_{m+1}\to 1$, Φ_1 and $\Phi_2\to 0$, we obtain

$$f_M^{n+1/2}+\theta f_\alpha\approx f_M^{n+1/2}\left\{\begin{array}{l}1+\left[1-\dfrac{\Delta t}{2\mu/p}\right]\dfrac{1}{2pT}\boldsymbol{\sigma}^{(1)}:\left(\mathbf{C}\otimes\mathbf{C}-\dfrac{1}{3}C^2\mathbf{I}\right)\\ +\left[1-\dfrac{\Delta t}{2\mu/p}\Pr\right]\dfrac{2}{5}\dfrac{1}{pT}\mathbf{C}\cdot\mathbf{q}^{(1)}\left(\dfrac{C^2}{2T}-\dfrac{5}{2}\right)\end{array}\right\}. \tag{3.15}$$

According to Ref. [32], the positivity of above PDF can be estimated by the coefficients before the second and third terms on the right-hand side of Eq. (3.15). Similarly, a parameter B refers to the maximum of these coefficients is defined as

$$B=\max\left(\left|\left[1-\frac{\Delta t}{2\mu/p}\right]\frac{\boldsymbol{\sigma}^{(1)}}{p}\right|,\left|\left[1-\frac{\Delta t}{2\mu/p}\Pr\right]\frac{\mathbf{q}^{(1)}}{pT^{1/2}}\right|\right). \tag{3.16}$$

If $B<0.1$, the PDF given by Eq. (3.15) is negative about 0.05% of the time [32]. Using Eq. (2.9), the range of parameter B satisfies

$$B<\left|1-\frac{\Delta t}{2\mu/p}\right|\frac{\mu}{p}\left(Ma+1\right)\approx\frac{\Delta t}{2}\left(Ma+1\right). \tag{3.17}$$

Applying the CFL condition, $\Delta t\left(Ma+1\right)/2=CFL\cdot\Delta h/2$. It is noted that, if setting the CFL number with $CFL\leq 1$ and the dimensionless cell size Δh much smaller than 1, the condition $B<0.1$ can be achieved in most situations.

In the kinetic limit, as $\beta\Delta t/\varepsilon\ll 1$, the Taylor expansion of $\left(f_M^{n+1/2}+\theta f_\alpha\right)$ is given as

$$f_M^{n+1/2}+\theta f_\alpha\approx f_M^{n+1/2}\left\{\begin{array}{l}1+O\left(\dfrac{\Delta t}{\mu/p}\right)\dfrac{1}{2pT}\boldsymbol{\sigma}^{(1)}:\left(\mathbf{C}\otimes\mathbf{C}-\dfrac{1}{3}C^2\mathbf{I}\right)\\ +O\left(\dfrac{\Delta t}{\mu/p}\right)\dfrac{2}{5}\dfrac{1}{pT}\Pr\mathbf{C}\cdot\mathbf{q}^{(1)}\left(\dfrac{C^2}{2T}-\dfrac{5}{2}\right)\end{array}\right\}. \tag{3.18}$$

Similar to Eq. (3.17), the estimation of parameter B is $B<\Delta t\left(Ma+1\right)$, which also assures the positivity of $\left(f_M^{n+1/2}+\theta f_\alpha\right)$. In addition, the scaling factor θ will not affect the other properties of the AAP-TRMC method, such as the preserving and accurate asymptotics, as discussed below.

3.2.2. Accuracy

In the fluid limit as $\beta\Delta t/\varepsilon\gg 1$, using Eqs. (3.5)–(3.9), the numerical solution of the AAP-TRMC collision operator approaches

$$\mathcal{C}_{\Delta t}^{AAP-TRMC}\left(f^*\right)=f_M^{n+1/2}+f^{n+1/2,(1)}+\frac{\Delta t}{2\varepsilon}Q^{(1)}\left(f^{n+1/2}\right). \tag{3.19}$$

Since the Strang splitting scheme (3.1) can also be written as $\mathcal{T}_{\Delta t/2}\left(f^n\right)=\mathcal{T}_{\Delta t}\left\{\mathcal{C}_{\Delta t}^{AAP-TRMC}\left[\mathcal{T}_{\Delta t/2}\left(f^{n-1}\right)\right]\right\}$, then combining Eqs. (3.7) and (3.19), we obtain

$$\begin{aligned}&\left[f_M^{n+1/2}+f^{n+1/2,(1)}\right]\left(\mathbf{V};\mathbf{x}\right)-\left[f_M^{n-1/2}+f^{n-1/2,(1)}\right]\left(\mathbf{V};\mathbf{x}-\mathbf{V}\Delta t\right)\\ &\qquad=\frac{\Delta t}{2\varepsilon}Q^{(1)}\left(f^{n+1/2}\right)\left(\mathbf{V};\mathbf{x}\right)+\frac{\Delta t}{2\varepsilon}Q^{(1)}\left(f^{n-1/2}\right)\left(\mathbf{V};\mathbf{x}-\mathbf{V}\Delta t\right),\end{aligned} \tag{3.20}$$

which is just the Crank-Nicolson scheme, therefore second order of accuracy can be achieved. The proof below is derived following the accuracy analysis of the standard TRMC method in Section 2.3, i.e., Eqs. (2.23)–(2.30). First, using Eq. (3.20), the solution of the macroscopic variables at the middle of the time step is calculated as

$$
\begin{aligned}
U_{AAP-TRMC}^{n+1/2} &= \left\langle \phi(\mathbf{V}) \left\{ \left[f_M^{n+1/2} + f^{n+1/2,(1)} \right] (\mathbf{V};\mathbf{x}) - \frac{\Delta t}{2\varepsilon} Q^{(1)} \left(f^{n+1/2} \right) (\mathbf{V};\mathbf{x}) \right\} \right\rangle \\
&= \left\langle \phi(\mathbf{V}) \left\{ \left[f_M^{n-1/2} + f^{n-1/2,(1)} \right] (\mathbf{V};\mathbf{x}-\mathbf{V}\Delta t) + \frac{\Delta t}{2\varepsilon} Q^{(1)} \left(f^{n-1/2} \right) (\mathbf{V};\mathbf{x}-\mathbf{V}\Delta t) \right\} \right\rangle.
\end{aligned} \tag{3.21}
$$

Taking Taylor expansion of Eq. (3.21) at time $(n-1/2)\Delta t$ and position $\mathbf{x}$ and using Chapman-Enskog theory, we have

$$
\begin{aligned}
U_{AAP-TRMC}^{n+1/2} &= \left\langle \phi(\mathbf{V}) f_M^{n-1/2}(\mathbf{V};\mathbf{x}) \right\rangle - \Delta t \frac{\partial}{\partial x} \left\langle \mathbf{V}\phi(\mathbf{V}) f_M^{n-1/2}(\mathbf{V};\mathbf{x}) \right\rangle \\
&\quad + \frac{\Delta t^2}{2} \frac{\partial^2}{\partial x^2} \left\langle \mathbf{V}^2 \phi(\mathbf{V}) f_M^{n-1/2}(\mathbf{V};\mathbf{x}) \right\rangle - \frac{\Delta t^2}{2\varepsilon} \frac{\partial}{\partial x} \left\langle \mathbf{V}\phi(\mathbf{V}) Q^{(1)} \left(f^{n-1/2} \right) (\mathbf{V};\mathbf{x}) \right\rangle + O(Kn) + O(\Delta t^3).
\end{aligned} \tag{3.22}
$$

Then, assuming the macroscopic variables also satisfy Euler equations, Taylor expansion of the solution $U^{n+1/2}$ at time step $(n-1/2)\Delta t$ and position $\mathbf{x}$ is given by Eq. (2.27). Comparing Eqs. (3.22) and (2.27), the numerical solution of the AAP-TRMC method yields

$$
U_{AAP-TRMC}^{n+1/2} = U^{n+1/2} + O(Kn) + O(\Delta t^3). \tag{3.23}
$$

Therefore, the AAP-TRMC method has second order of accuracy in time in the fluid limit.

In the kinetic limit, as shown in Eq. (3.18), the additional PDF θf_α approaches to $A_{m+1} O(\beta \Delta t/\varepsilon)$, which is negligible compared to the other terms in the standard TRMC method. Therefore, the AAP-TRMC scheme reduces to standard TRMC method and shares the same accuracy in the kinetic limit.

3.2.3. Asymptotic preserving property

In the fluid limit, as $\beta \Delta t/\varepsilon \gg 1$, the approximate solution of the AAP-TRMC collision operator is given by Eq. (3.19). Then, applying the convection operator for another half of time step, the numerical solution at time $(n+1)\Delta t$ can be written as

$$
\begin{aligned}
f^{n+1} &= \mathcal{T}_{\Delta t/2} \left\{ \mathcal{C}_{\Delta t}^{AAP-TRMC} \left(f^* \right) \right\} = \left[f_M^{n+1/2} + f^{n+1/2,(1)} + \frac{\Delta t}{2\varepsilon} Q^{(1)} \left(f^{n+1/2} \right) \right] (\mathbf{V};\mathbf{x}-\mathbf{V}\Delta t/2) \\
&= f_M^{n+1/2}(\mathbf{V};\mathbf{x}) + f^{n+1/2,(1)}(\mathbf{V};\mathbf{x}) + \frac{\Delta t}{2} \frac{\partial f_M^{n+1/2}(\mathbf{V};\mathbf{x})}{\partial t} + O(\Delta t^2).
\end{aligned} \tag{3.24}
$$

Obviously, the AAP-TRMC method preserves the Navier-Stokes asymptotics.

3.3. The numerical implementation

In summary, the AAP-TRMC method employs the Strang splitting scheme as shown Eq. (3.1), with a newly proposed collision operator as

$$
\mathcal{C}_{\Delta t}^{AAP-TRMC}(f^*) = \sum_{k=0}^{m} A_k f_k + A_{m+1} \left(f_M^{n+1/2} + \theta f_\alpha \right). \tag{3.25}
$$

Similar to the standard TRMC method, its computational procedure includes following five steps:

1. **Initialization**. Assign simulated particles in the computational domain;
2. **Convection**. Compute particle motions for the first half time step;
3. **Collision**. Compute particle collisions for a whole time step;
4. **Convection.** Compute particle motions for another half time step;
5. **Sampling.** Compute the macroscopic quantities.

We give details of above numerical implementations below.

3.3.1. Initialization

Similar to DSMC, the AAP-TRMC method employs stochastic particles to simulate the PDF of gas molecules. In each compactional cell, the number of initial particles N_c is determined as

$$
N_c = Iround \left(\frac{nV_c}{F_N} \right), \tag{3.26}
$$

and

$$Iround\,(z) = \begin{cases} [z] & \text{with probability } [z]+1-z, \\ [z]+1 & \text{with probability } z-[z], \end{cases} \tag{3.27}$$

where $[z]$ refers to the integer part of z. n is the number density; V_c is the cell volume; and F_N refers to the number of real molecules represented by one computational particle.

For each computational particle with index α, its velocity $\mathbf{M}^{(\alpha)}$ is sampled from the local equilibrium distribution, i.e., the Maxwellian distribution as shown in Eq. (2.7), and its position $\mathbf{X}^{(\alpha)}$ is randomly distributed in the computational cell.

3.3.2. Convection

Particle' position is updated according to its velocity for half time step $\Delta t/2$, e.g., for the convection of the first half time step, we obtain

$$\mathbf{X}^{(\alpha),n+1/2} = \mathbf{X}^{(\alpha),n} + \mathbf{M}^{(\alpha),n}\Delta t/2. \tag{3.28}$$

The boundary condition of the AAP-TRMC method is as same as DSMC, and also implemented in the convection process.

3.3.3. Collision

In general, the collision operator of the AAP-TRMC method is implemented similarly to the standard TRMC scheme. To emphasizing the difference between these two methods, only a brief procedure of the second order AAP-TRMC method with VHS molecules is presented below. However, the details of the collision algorithm for the TRMC method are referred to Ref. [14].

Algorithm 3.1 *(Collision operator of AAP-TRMC2 for VHS molecules).* For each computational cell:

1) Determining the parameter β. Compute an upper bound of $(\sigma_T c_r)_{\max}$, $\sigma_T = \int_{\mathbb{S}^2}\sigma d\Omega$ is the total collision cross-section. The parameter β in the AAP-TRMC method is chosen as $\rho\,(\sigma_T c_r)_{\max}$ [14];
2) Computing A_0, A_1, A_2 and A_3 according to Eq. (2.19), and Φ_1 and Φ_2 according to Eq. (3.13);
3) Randomly selecting three groups of particles from the computational cell corresponding to the last three terms in the right-hand side of Eq. (3.12), respectively. Setting $N_1 = Iround(A_1 N_c)$, $N_2 = Iround(A_2 N_c)$ and $N_3 = Iround(A_3 N_c)$, which are the number of particles in each group;
4) The first group of particles performs the collision process according to the collision term $P\,(f^*, f^*)\,/\beta$;
5) The second group of particles performs the collision process according to the collision term $P\,(f^*, f_1)\,/\beta$. The algorithm of computing these two collision terms for VHS molecules is as same as Ref. [14];
6) Resampling the velocities of the third group of particles according to $\left(f_M^{n+1/2} + \theta f_\alpha\right)$, where $f_M^{n+1/2}$ and f_α are given as Eq. (2.7) and Eq. (3.9), respectively. It is noted that both $f_M^{n+1/2}$ and f_α are determined by the macroscopic quantities, such as ρ, $\mathbf{u}$ and T, after the convection step of the first half time step. Its sampling method is introduced in section 3.3.4.

The implementations of the other AAP-TRMC schemes, such as the first order one, i.e., AAP-TRMC1, can be performed similarly.

3.3.4. Sampling

Like DSMC, the macroscopic quantities are averaged from the velocities of the computational particles as

$$\rho = mN_c/V_c,\ u_i = \sum_{k=1}^{N_c} M_i^{(k)}/N_c \quad \text{and} T = \sum_{k=1}^{N_c}\left(M_i^{(k)} - u_i\right)^2/3R\,(N_c-1)\,, \tag{3.29}$$

where the factor $1/(N_c-1)$ in the temperature occurs to produce unbiasedness of T. To reduce statistical noise, the exponentially weighted moving time averaging [33] is employed for the simulation of steady flows. In addition, as the AAP-TRMC method has a second-order of accuracy in time in the fluid limit, a same order accuracy should be achieved in space. Therefore, at least a second order interpolation is requested in the AAP-TRMC method. Then, the Maxwellian distribution $f_M(\mathbf{V}; \mathbf{X}^{(\alpha)}, t)$ and the additional PDF $f_\alpha(\mathbf{V}; \mathbf{X}^{(\alpha)}, t)$ related to the resampled computational particles are computed based on the macroscopic quantities and their derivatives at the particle location $\mathbf{X}^{(\alpha)}$.

The molecular velocities satisfied PDF $\left(f_M^{n+1/2} + \theta f_\alpha\right)$ can be sampled using either the acceptance-rejection algorithm [32] or the Metropolis-Hastings (MH) method [34].

3.3.5. Conservation

As well Known, if the molecular velocities are sampled by the acceptance-rejection algorithm or the MH method, the momentum and energy conservation can only be obtained in a statistical sense. Therefore, like other stochastic particle

methods [38,39], to conserve the momentum and energy in each cell, a correction step for the velocities of individual particle is implemented after the collision step, i.e.,

$$\mathbf{M}^{(k)} = \alpha \left(\mathbf{M}^{(k)'} - \sum_{k=1}^{N_c} \mathbf{M}^{(k)'} / N_c \right) + \sum_{k=1}^{N_c} \mathbf{M}^{(k)*} / N_c, \tag{3.30}$$

where $\mathbf{M}^{(k)*}$ and $\mathbf{M}^{(k)'}$ are the velocities of the k$^{\text{th}}$ particle before and after the collision step, respectively. The coefficient α is given by

$$\alpha = \sqrt{\sum_{k=1}^{N_c} \left(M_i^{(k)*} - \sum_{k=1}^{N_c} M_i^{(k)*} / N_c \right)^2 / \sum_{k=1}^{N_c} \left(M_i^{(k)'} - \sum_{k=1}^{N_c} M_i^{(k)'} / N_c \right)^2}. \tag{3.31}$$

4. Numerical results

4.1. Poiseuille flow

The Poiseuille flow is first calculated. The argon gas, initially in the standard condition ($T_0 = 273$ K and $p_0 = 1$ atm), is simulated with three Kn numbers varied from the rarefied to the continuum flow regimes, such as 0.1, 0.01 and 0.001. The distance H between parallel walls is calculated based on the Kn number, i.e., $H = \lambda/\text{Kn}$, where $\lambda = 6.36 \times 10^{-8}$ m. The wall temperature keeps 273 K and fully diffusive boundary condition is employed. For three Kn numbers, corresponding pressure gradients are chosen as 4.0×10^{10} Pa m^{-1}, 4.0×10^{8} Pa m^{-1} and 4.0×10^{6} Pa m^{-1}, respectively.

The VHS molecules are employed and the molecular diameter is set as 4.17×10^{-10} m with a reference temperature $T_{ref} = 273$ K and viscosity $\mu_{ref} = 2.117 \times 10^{-5}$ Pa s. With the exponent $\omega = 0.81$, the viscosity of argon is calculated as $\mu = \mu_{ref} \left(T/T_{ref} \right)^{\omega}$. In this case, computational cells are uniformly distributed with a cell width Δh. The time step is determined by the CFL condition with $CFL = 1.0$.

Fig. 1 shows the mean velocity and temperature distributions calculated by the AAP-TRMC2 method. From Fig. (1a) to (1f), 100, 60, and 140 computational cells are employed for Kn = 0.1, 0.01, and 0.001, respectively. 500 computational particles are assigned in each cell initially. For large Kn numbers, i.e., 0.1 and 0.01, the results of AAP-TRMC2 agree well with the DSMC data. However, larger cell and time size can be used in AAP-TRMC2. For the smaller Kn number of 0.001, the gas flow belongs to the continuum regime and DSMC is computationally expansive. The AAP-TRMC2 method is compared with the analytical NS solution [37], and consistent results are also obtained.

To investigate the accuracy of the AAP-TRMC method in different flow regions, we calculate the L_2-norm of error for the mean velocity as shown in Fig. 2, in which u_x^{ref} denotes the finest DSMC results for Kn = 0.1 and 0.01 and the analytical NS solutions for Kn = 0.001. In the kinetic limit, such as Kn = 0.1, AAP-TRMC reduces to the standard TRMC method. Therefore, the curves of TRMC2, which refers to the second order standard TRMC method, and AAP-TRMC2 overlap with each other. However, the first order AAP-TRMC method shows less accurate than AAP-TRMC2. In the fluid limit, such as Kn = 0.001, both of the AAP-TRMC1 and AAP-TRMC2 methods turn to the Crank-Nicolson scheme and achieve the second order of accuracy. Conversely, larger numerical dissipation is observed for the standard TRMC scheme in the fluid limit, and its accuracy approaches to the first order as shown in Sec. 2.3.2. For the moderate Knudsen number, such as Kn = 0.01, the AAP-TRMC method can be considered as a mixture of the standard TRMC and Crank-Nicolson schemes. Therefore, due to the competition of these two schemes, a flat error curve is observed in this range. Even so, it is still noted that the AAP-TRMC method is more accurate than the standard TRMC method with the moderate Knudsen number.

In addition, the computational efficiency of the AAP-TRMC2 method is compared with DSMC [1] for the case of Kn = 0.001. Since the accuracy of the stochastic particle method is also dependent on the number of computational particles, three particle numbers are tested for the AAP-TRMC2 method, i.e., 50, 200 and 500 particles per cell. In DSMC, we initially assigned 50 particles in each cell. In Fig. 3, different levels of error are achieved by changing mesh size, and the CFL number is also set as 1.0 for all simulations. The computational time refers to the cost CPU time to simulate the Poiseuille flow for a certain physical period. It is normalized by T_0, which is the longest computational time among the DSMC cases. We note that, to obtain the same level of accuracy for this one-dimensional flow, the AAP-TRMC2 method can save at least 10 times the CPU time compared to DSMC. It is also noted that the accuracy of the AAP-TRMC2 method decreases as fewer computational particles are employed. However, even if 50 particle per cell is used, the AAP-TRMC2 still demonstrates better performance than DSMC.

4.2. Sod tube flow

The Sod tube flow is a typical multiscale one-dimensional gas flow. In this test, the computational domain is set as one meter and a density discontinuity is initially assigned in the middle of the tube. Argon gas is simulated and the VHS molecule model as same as Sec. 4.1 is employed. At the beginning, the mean velocity is zero and the gaseous temperature is 273 K in the whole tube. However, the densities in the left and right sides of the tube are different. Three Kn numbers,

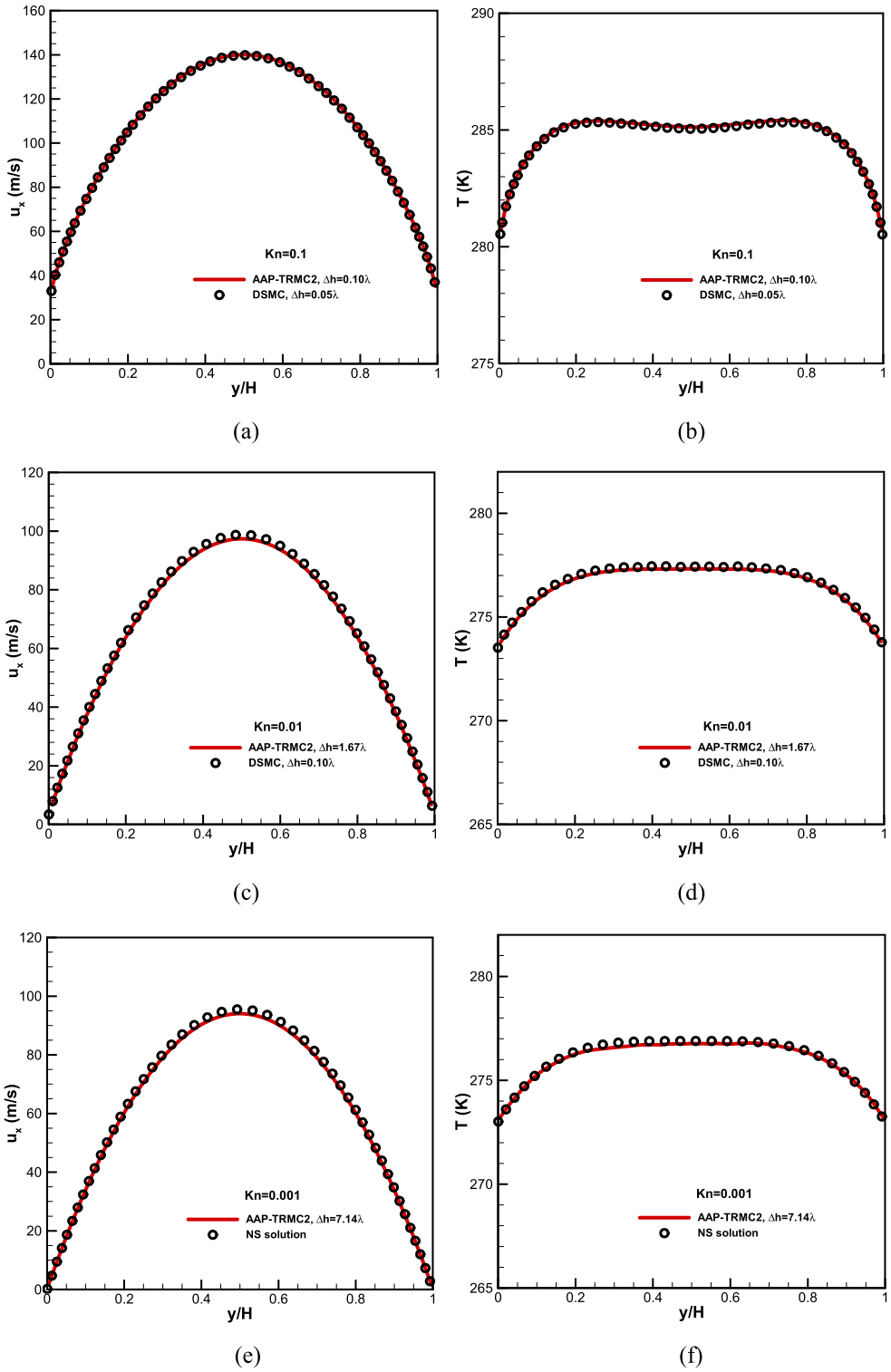

Fig. 1. Comparison of the mean velocity and temperature distributions of the Poiseuille flows calculated by the AAP-TRMC2 method, DSMC and the NS solutions for Knudsen numbers of 0.1, 0.01 and 0.001, respectively.

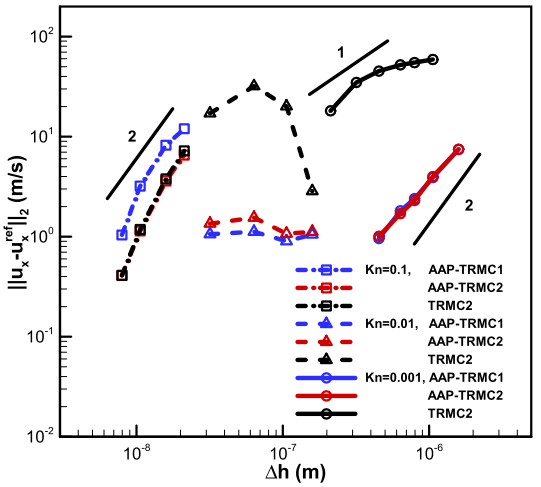

Fig. 2. L_2-norm of error of the mean velocity in Poiseuille flows for Knudsen numbers of 0.1, 0.01 and 0.001, respectively. The results of the first and second order AAP-TRMC methods and the original second order TRMC are compared.

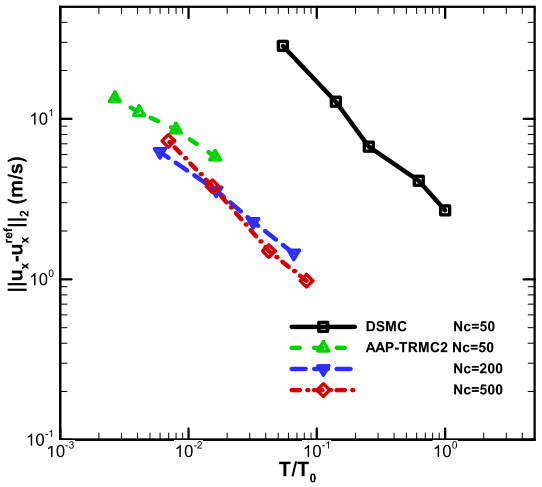

Fig. 3. L_2-norm of error of the mean velocity versus computational time in Poiseuille flows with Kn = 0.001. T_0 is the longest computational time taken by DSMC. Initially, the AAP-TRMC2 method employs 50, 200 and 500 particles per cell, respectively, and 50 particles are assigned for the DSMC method.

Table 1
Computational parameters for the Sod tube flow.

Case	Left density ρ_L (kg m^{-3})	Right density ρ_R (kg m^{-3})	Cell number		Knudsen number
			AAP-TRMC	DSMC	
1	1.0×10^{-5}	0.125×10^{-5}	200	500	1.125×10^{-2}
2	1.0×10^{-4}	0.125×10^{-4}		2000	1.125×10^{-3}
3	1.0×10^{-3}	0.125×10^{-3}		20000	1.125×10^{-4}

which are dependent on the initial mean free path of the right chamber and the length of the tube, varied from 10^{-4} to 10^{-2} are calculated and corresponding densities are given in Table 1. The first and second order AAP-TRMC method are validated and compared with DSMC. 200 uniform computational cells are used for all simulations of AAP-TRMC, however much more cells are applied for DSMC. The time step is determined by the CFL condition with $CFL = 0.5$. The flow field is evolved up to the time $t_{\text{final}} = 5.0 \times 10^{-4}$ s. For the unsteady flow, to avoid the influence of the statistical noise, a large number of computational particles are employed here, i.e., around 2.4×10^4 and 1.9×10^5 initial particles for the right and left sides, respectively.

Fig. 4 shows the density distribution for three cases. It is noted that both the AAP-TRMC1 and AAP-TRMC2 schemes provide consistent results compared to the reference data calculated by DSMC. Fig. 5 presents the heat flux of the Sod tube flow. Although AAP-TRMC employs less computational cells, their heat fluxes agree well with DSMC even in the continuum

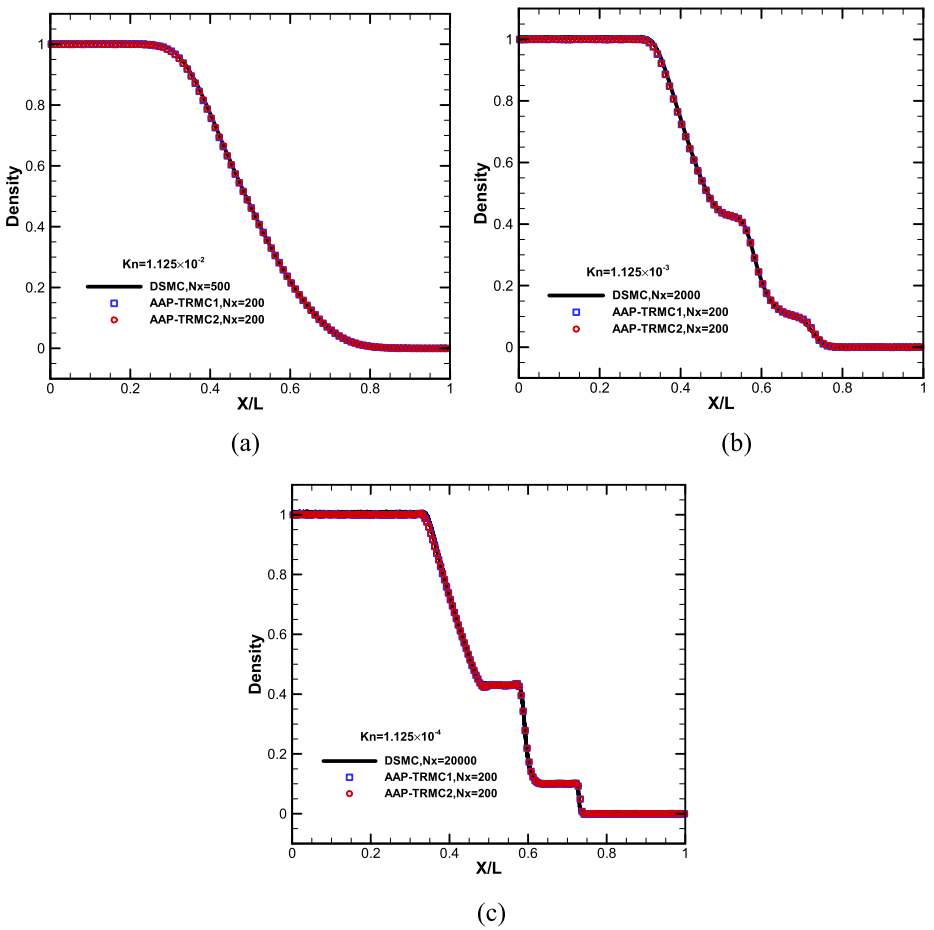

Fig. 4. Comparison of the density distribution $(\rho - \rho_R)/(\rho_L - \rho_R)$ of the Sod tube flows calculated by the AAP-TRMC and DSMC methods for $\mathrm{Kn} = 1.125 \times 10^{-2}$, 1.125×10^{-3} and 1.125×10^{-4}, respectively.

Table 2
Computational parameters for the shock wave flow.

Case		Number density (m^{-3})	Temperature (K)	Mach number
1	Pre-shock	1.6095×10^{21}	300	2.0
	Post-shock	3.679×10^{21}	623	
2	Pre-shock	1.6095×10^{21}	300	15.0
	Post-shock	6.353×10^{21}	21357	

flow regime, i.e., $\mathrm{Kn} = 1.125 \times 10^{-4}$. It is attributed to the asymptotic preserving of NS equations and asymptotic accurate properties for the AAP-TRMC method.

4.3. Shock wave

In this section, the shock wave flows of argon gas at Ma = 2 and Ma = 15 are simulated. For both Mach numbers, the temperature and number density of the free stream are 300 K and 1.6095×10^{21} m^{-3}, respectively. The computational domain is 100λ, where $\lambda = 1.094 \times 10^{-3}$ m is the mean free path based on the free stream condition. The other computational parameters are given in Table 2. 500 uniform cells are employed for DSMC; however, three types of grids are applied for the AAP-TRMC method to investigate its accuracy, such as 50, 100 and 200 uniform cells. The CFL number is set as $CFL = 0.5$ for all simulations. The VHS model is also used as Sec. 4.1. Initially, 500 computational particles are assigned in each cell ahead of the shock wave.

Figs. 6 and 7 compare the temperature and density profiles for Ma = 2 and Ma = 15 cases, where the temperature and density are normalized as $(T - T_L)/(T_R - T_L)$ and $(\rho - \rho_L)/(\rho_R - \rho_L)$, respectively. T_L, ρ_L and T_R, ρ_R denote the

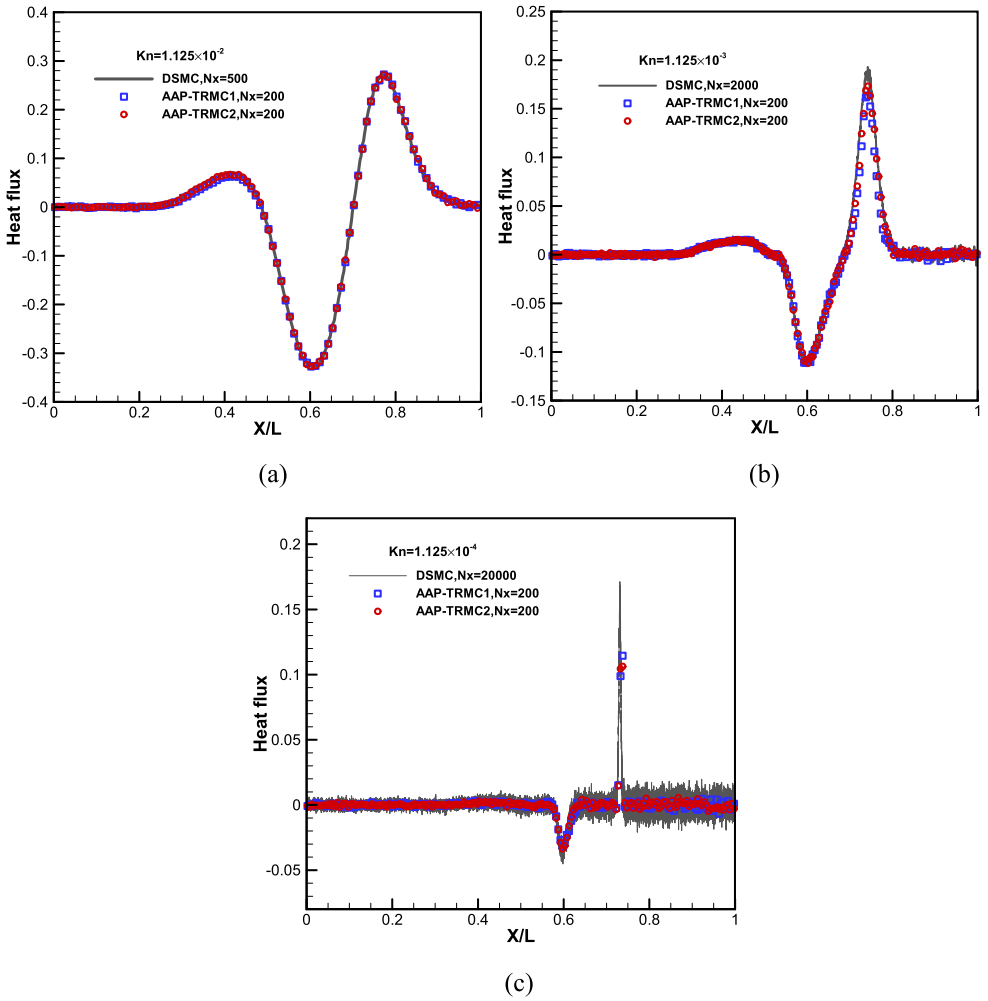

Fig. 5. Comparison of the normalized heat flux $q/p\sqrt{RT}$ of the Sod tube flows calculated by the AAP-TRMC and DSMC method for $\mathrm{Kn} = 1.125 \times 10^{-2}$, 1.125×10^{-3} and 1.125×10^{-4}, respectively. q is heat flux, and p and T refer to the pressure and temperature.

Table 3
Inflow conditions for the hypersonic flows past cylinder.

Case	Number density (m^{-3})	Temperature (K)	Velocity (m/s)	Kn number
1	4.247×10^{20}	200	2624	0.01
2	1.699×10^{19}			0.25

temperature and density before and after the shock wave as shown in Table 2. For the small Mach number, in Fig. 6 the results of AAP-TRMC1 and AAP-TRMC2 are similar with each other and both of them approach the DSMC data as the cell number increases. For the large Mach number, as AAP-TRMC2 is more accurate than AAP-TRMC1 in the kinetic limit, in Fig. 7, the second order AAP-TRMC method presents better performance than the first order scheme. Additionally, the results of both AAP-TRMC schemes also agree well with the DSMC data as cell size decreases.

4.4. The hypersonic flows past a cylinder

Hypersonic flows past a cylinder are investigated in this section. The results of the AAP-TRMC method are compared with the DSMC data provided by Lofthouse in Ref. [35]. In this test, the cylinder diameter is 0.3048 m. The temperature of the cylinder surface keeps 500 K, and fully diffusive wall condition is employed. Argon gas flows with two Knudsen numbers, i.e., $\mathrm{Kn} = 0.25$ and $\mathrm{Kn} = 0.01$, are simulated. The detailed inflow conditions are presented in Table 3. The computational domain is a rectangular box, i.e., 3.2×1.6 m^2 for $\mathrm{Kn} = 0.25$ and 1.6×0.8 m^2 for $\mathrm{Kn} = 0.01$, respectively. In addition, Cartesian grids with refinement around the cylinder are employed to discretize the physical space as shown in Fig. 8. The

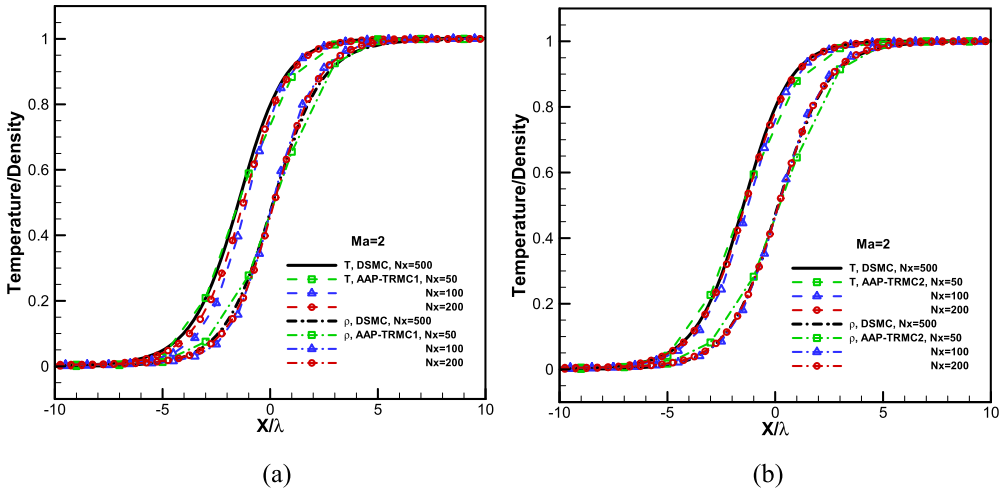

Fig. 6. Comparison of the temperature and density profiles of the shock wave at Ma = 2 between (a) AAP-TRMC1, (b) AAP-TRMC2 and the reference data calculated by DSMC. The computational parameters are given in Table 2.

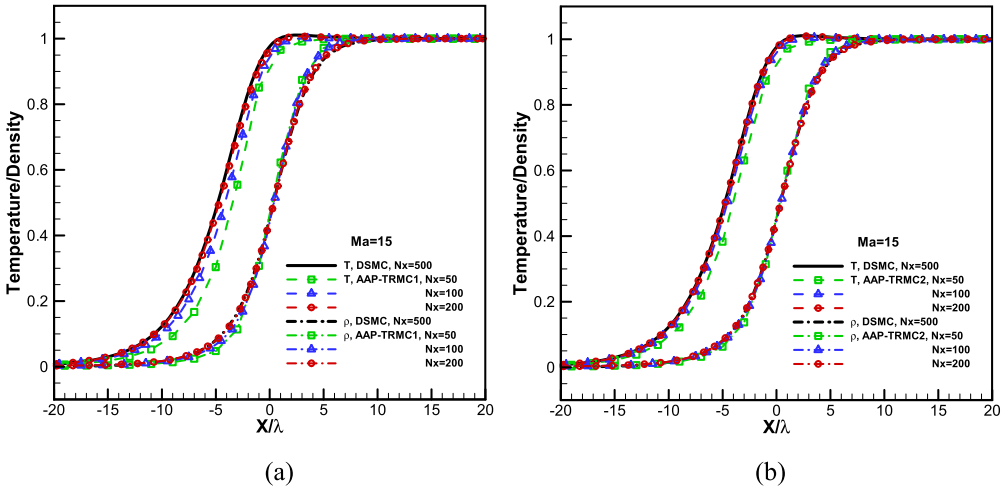

Fig. 7. Comparison of the temperature and density profiles of the shock wave at Ma = 15 between (a) AAP-TRMC1, (b) AAP-TRMC2 and the reference data calculated by DSMC. The computational parameters are given in Table 2.

cell numbers of the coarsest level are set to be 200×100 for all simulations. The CFL condition is employed with $CFL = 0.3$. At the beginning, all of the computational cells are initialized with the inflow conditions, and 200 computational particles are assigned in every coarsest cell. In addition, the VHS model is used. A reference diameter of 3.595×10^{-10} m is chosen at the reference temperature 1000 K and the reference viscosity is 5.07×10^{-5} Pa s with an exponent $\omega = 0.734$.

Fig. 8 also depicts the density distribution around the cylinder. It is noted that the gas flow is compressed in front of the cylinder and expanded after it. Therefore, the flow field, which transits from the continuum regime to the rarefied regime around the cylinder, is a typical multi-scale problem. The flow properties are determined by both the Mach and Knudsen numbers. As the Kn number increases, the shock wave ahead of the cylinder becomes thicker as shown in Fig. 8. Moreover, Fig. 9 shows the temperature predicted along the stagnation line in front of the cylinder. The results of AAP-TRMC2 are consistent with the DSMC data in Ref. [35] for Kn = 0.25 and Kn = 0.01. However, at Kn = 0.01 the results of the standard TRMC2 method depart from the reference data due to its huge numerical dissipation in the fluid limit.

In Fig. 10, the surface friction and heating coefficients are defined by

$$C_F = \sigma_{sur} / \left(\rho_\infty u_\infty^2 / 2 \right) \quad \text{and} \quad C_H = q_{sur} / \left(\rho_\infty u_\infty^3 / 2 \right), \tag{4.1}$$

where σ_{sur} and q_{sur} are the shear stress and heat flux on the wall. ρ_∞ and u_∞ denote the density and mean velocity of the freestream, respectively. Fig. 10 compares the results of AAP-TRMC2 with the standard TRMC2 and DSMC methods for Kn = 0.25. It is noted that both TRMC schemes provide appropriate results. In contrast, as the Kn number decreases, i.e., for Kn = 0.01, the numerical solution in front of the cylinder tends to the fluid limit. Since the standard TRMC2 method

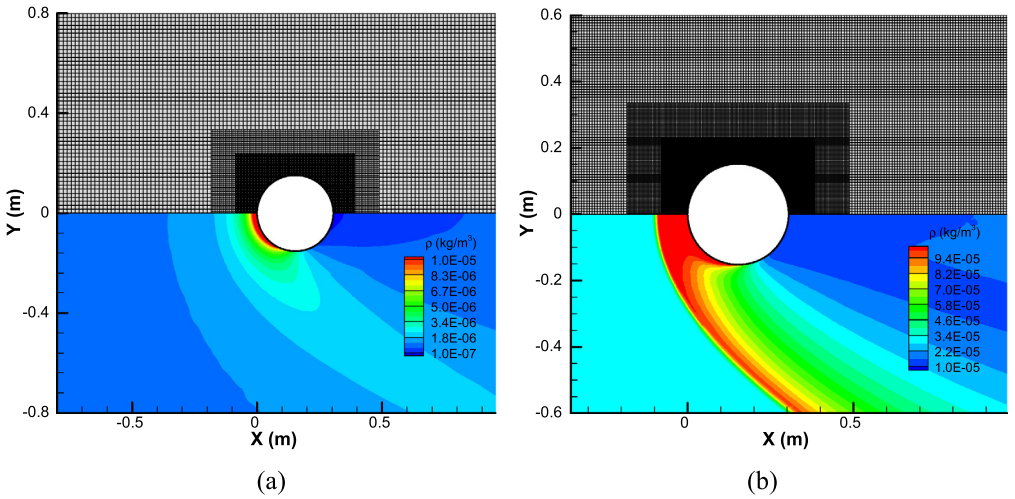

Fig. 8. Meshes and density distribution for a Mach 10 freestream flow past a cylinder at (a) Kn = 0.25 and (b) Kn = 0.01. Calculated by the AAP-TRMC2 method with 200 × 100 grids (coarsest level). The computational parameters are given in Table 3.

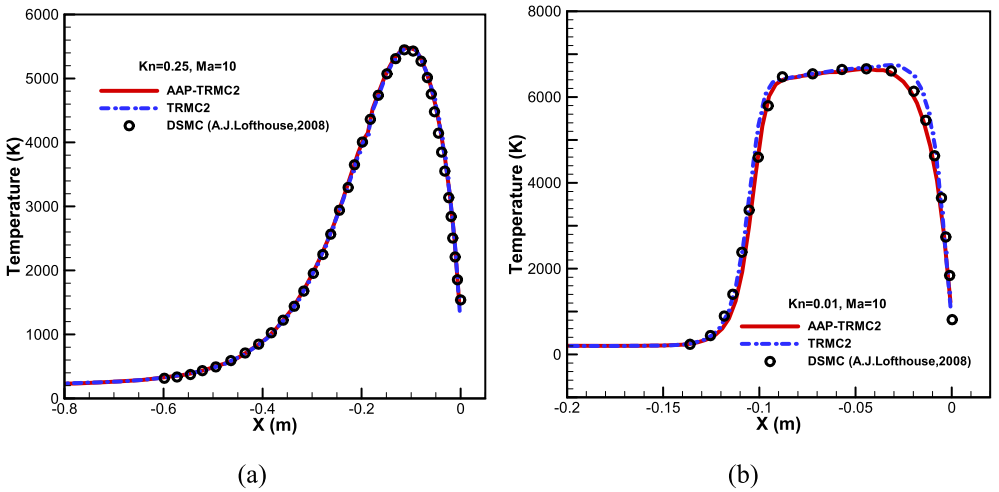

Fig. 9. Temperature distribution along the stagnation line for a Mach 10 freestream flow past a cylinder with (a) Kn = 0.25 and (b) Kn = 0.01. The solid and dash-dotted lines represent the results of the AAP-TRMC2 and standard TRMC2 methods with 200 × 100 grids (coarsest level) and the symbols refer to the DSMC data in Ref. [35].

preserves the Euler equations and only has first order accuracy in the fluid limit, it will significantly underestimate the shear stress and heat flux on the surface as shown in Fig. 11. However, the proposed AAP-TRMC2 method shows consistent results with DSMC. Therefore, benefitting from higher order of accuracy in the fluid limit, the AAP-TRMC method can use less computational cell and time than the standard TRMC method, and should be more efficient when simulating multi-scale gas flows.

5. Conclusion

In this paper, a new time relaxed Monte Carlo method is proposed. In the kinetic limit, it is consistent with the standard TRMC method. However, by introducing a micro-macro decomposition for the TRMC collision operator and a suitable time discretization, this new proposed TRMC method can preserve the Navier-Stokes asymptotics and second order accurate in the fluid limit. Therefore, less numerical dissipation and higher computational efficiency are obtained when simulating multi-scale gas flows. In addition, compared to the domain decomposition methods, the present TRMC scheme can be considered as a hybrid scheme in the view point of algorithms instead of the physical domain. Thus, without an actual interface between different solvers, the transition from the continuum to rarefied flow regimes can be captured much more smoothly and more accurately. It is also noted that, although this framework is applied to TRMC in this work, extending it to the other asymptotic preserving Monte Carlo schemes, such as the exponential Runge–Kutta [15] and asymptotic-preserving Monte Carlo method [16], is also possible. Moreover, combining the solution of DSMC and continuous model, this strategy

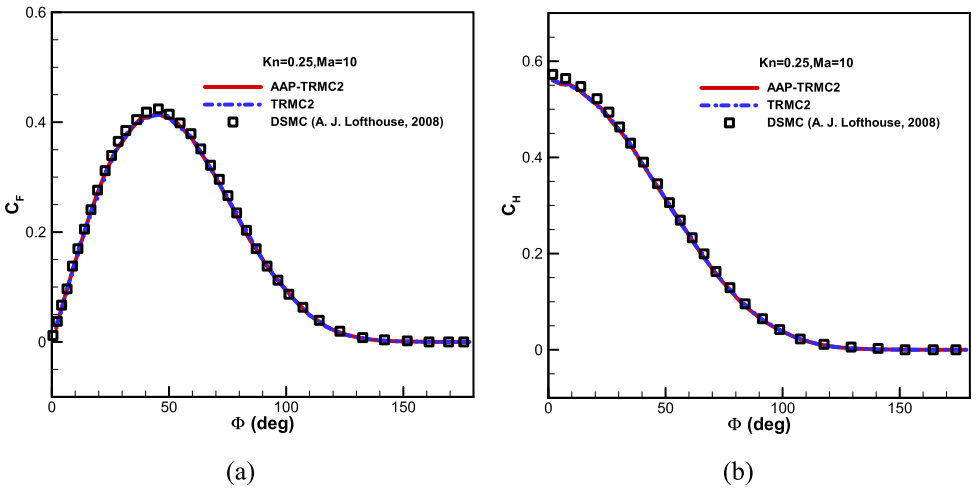

Fig. 10. Surface (a) friction and (b) heating coefficients for a hypersonic flow past a cylinder at Ma = 10 and Kn = 0.25. The solid and dash-dotted lines represent the results of the AAP-TRMC2 and standard TRMC2 methods with 200 × 100 grids (coarsest level) and the symbols refer to the DSMC data in Ref. [35].

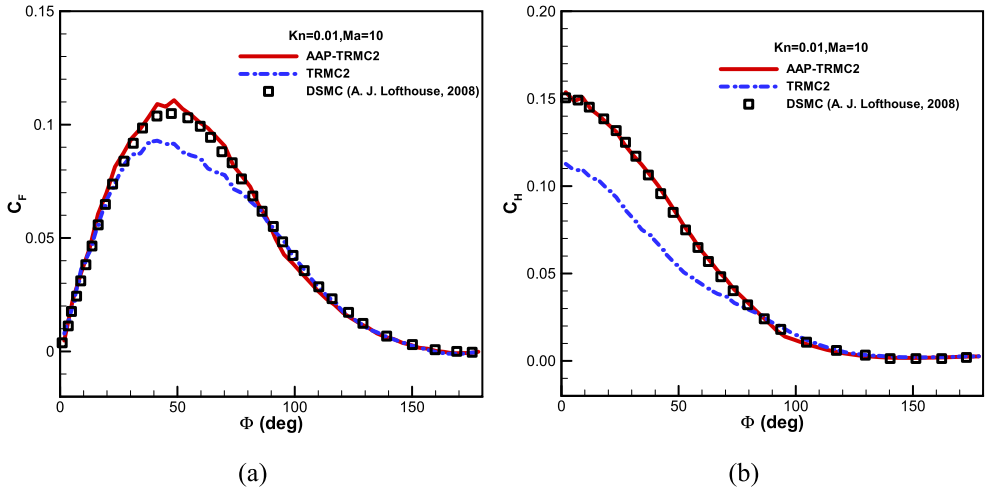

Fig. 11. Surface (a) friction and (b) heating coefficients for a hypersonic flow past a cylinder at Ma = 10 and Kn = 0.01. The solid and dash-dotted lines represent the results of the AAP-TRMC2 and standard TRMC2 methods with 200 × 100 grids (coarsest level) and the symbols refer to the DSMC data in Ref. [35].

can directly succeed the advantages and knowledge of existing DSMC and continuous models, therefore, it may be much easier applied to develop a multi-scale scheme for complex gases, such as multi-species. This work will be done in the future.

CRediT authorship contribution statement

Fei Fei: Conceptualization, Formal analysis, Methodology, Software, Validation, Writing – original draft.

Declaration of competing interest

The authors declare that they have no known competing financial interests or personal relationships that could have appeared to influence the work reported in this paper.

Data availability

Data will be made available on request.

Acknowledgements

This work was supported by the National Natural Science Foundation of China (No. 51876076).

References

[1] G.A. Bird, Molecular Gas Dynamics and the Direct Simulation of Gas Flows, Oxford University Press, Clarendon, Oxford, 1994.
[2] Q. Sun, I.D. Boyd, G.V. Candler, A hybrid continuum/particle approach for modeling rarefied gas flows, J. Comput. Phys. 194 (2004) 256–277.
[3] T.E. Schwartzentruber, I.D. Boyd, A hybrid particle-continuum method applied to shock waves, J. Comput. Phys. 215 (2006) 402–416.
[4] T.E. Schwartzentruber, L.C. Scalabrin, I.D. Boyd, A modular particle–continuum numerical method for hypersonic non-equilibrium gas flows, J. Comput. Phys. 225 (2007) 1159–1174.
[5] H. Wijesinghe, N. Hadjiconstantinou, Discussion of hybrid atomistic-continuum methods for multiscale hydrodynamics, Int. J. Multiscale Comput. Eng. 2 (2004) 189–202.
[6] W.L. Wang, I.D. Boyd, Predicting continuum breakdown in hypersonic viscous flows, Phys. Fluids 15 (1) (2003) 91–100.
[7] J. Meng, N. Dongari, J.M. Reese, Y. Zhang, Breakdown parameter for kinetic modeling of multiscale gas flows, Phys. Rev. E 89 (6) (2014) 063305.
[8] A. Alamatsaz, A. Venkattraman, Characterizing deviation from equilibrium in direct simulation Monte Carlo simulations, Phys. Fluids 31 (4) (2019) 042005.
[9] F. Fei, H.H. Liu, Z.H. Liu, J. Zhang, A benchmark study of kinetic models for shock waves, AIAA J. 58 (6) (2020) 2596–2608.
[10] R. Kumar, E. Titov, D.A. Levin, Development of a particle–particle hybrid scheme to simulate multiscale transitional flows, AIAA J. 51 (1) (2012) 200–217.
[11] M.H. Gorji, P. Jenny, Fokker–Planck–DSMC algorithm for simulations of rarefied gas flows, J. Comput. Phys. 287 (2015) 110–129.
[12] F. Fei, P. Jenny, A hybrid particle approach based on the unified stochastic particle Bhatnagar-Gross-Krook and DSMC methods, J. Comput. Phys. 424 (2021) 109858.
[13] E. Gabetta, L. Pareschi, G. Toscani, Relaxation schemes for nonlinear kinetic equations, SIAM J. Numer. Anal. 34 (1997) 2168–2194.
[14] L. Pareschi, G. Russo, Time relaxed Monte Carlo methods for the Boltzmann equation, SIAM J. Sci. Comput. 23 (2001) 1253–1273.
[15] G. Dimarco, L. Pareschi, Exponential Runge–Kutta methods for stiff kinetic equations, SIAM J. Numer. Anal. 49 (2011) 2057–2077.
[16] W. Ren, H. Liu, S. Jin, An asymptotic-preserving Monte Carlo method for the Boltzmann equation, J. Comput. Phys. 276 (2014) 380–404.
[17] S. Jin, Efficient asymptotic-preserving (AP) schemes for some multiscale kinetic equations, SIAM J. Sci. Comput. 21 (1999) 441–454.
[18] M. Lemou, L. Mieussens, A new asymptotic preserving scheme based on micro-macro formulation for linear kinetic equations in the diffusion limit, SIAM J. Sci. Comput. 31 (1) (2008) 334–368.
[19] M. Bennoune, M. Lemou, L. Mieussens, Uniformly stable numerical schemes for the Boltzmann equation preserving the compressible Navier–Stokes asymptotics, J. Comput. Phys. 227 (1) (2008) 3781–3803.
[20] A. Crestetto, N. Crouseilles, G. Dimarco, M. Lemou, A new deviational Asymptotic Preserving Monte Carlo method for the homogeneous Boltzmann equation, Commun. Math. Sci. 18 (8) (2020) 2305–2339.
[21] L. Pareschi, S. Trazzi, Numerical solution of the Boltzmann equation by time relaxed Monte Carlo (TRMC) methods, Int. J. Numer. Methods Fluids 48 (2005) 947–983.
[22] E. Wild, On Boltzmann's equation in the kinetic theory of gases, Math. Proc. Camb. Philos. Soc. 47 (1950) 602–609.
[23] F. Fei, P. Jenny, A high-order unified stochastic particle method based on the Bhatnagar-Gross-Krook model for multi-scale gas flows, Comput. Phys. Commun. 274 (2022) 108303.
[24] F. Fei, J. Zhang, J. Li, Z.H. Liu, A unified stochastic particle Bhatnagar-Gross-Krook method for multiscale gas flows, J. Comput. Phys. 400 (2020) 108972.
[25] G. Dimarco, L. Pareschi, Numerical methods for kinetic equations, Acta Numer. 23 (2014) 369–520.
[26] K. Nanbu, Direct simulation scheme derived from the Boltzmann equation, J. Phys. Soc. Jpn. 49 (1980) 2042–2049.
[27] L. Pareschi, G. Russo, Asymptotic preserving Monte Carlo methods for the Boltzmann equation, Transp. Theory Stat. Phys. 29 (2000) 415–430.
[28] F. Filbet, G. Russo, High order numerical methods for the space non-homogeneous Boltzmann equation, J. Comput. Phys. 186 (2) (2003) 457–480.
[29] G. Strang, On the construction and the comparison of difference schemes, SIAM J. Numer. Anal. 5 (1968) 506–517.
[30] M.C. Ding, J.M. Qiu, R. Shu, Accuracy and stability analysis of the semi-Lagrangian method for stiff hyperbolic relaxation systems and kinetic BGK model, arXiv preprint, arXiv:2105.02974, 2021.
[31] S. Jin, Runge–Kutta methods for hyperbolic conservation laws with stiff relaxation terms, J. Comput. Phys. 122 (1995) 51–67.
[32] A.L. Garcia, B.J. Alder, Generation of the Chapman–Enskog distribution, J. Comput. Phys. 140 (1) (1998) 66–70.
[33] P. Jenny, M. Torrilhon, S. Heinz, A solution algorithm for the fluid dynamic equations based on a stochastic model for molecular motion, J. Comput. Phys. 229 (2010) 1077–1098.
[34] M. Pfeiffer, Particle-based fluid dynamics: comparison of different Bhatnagar-Gross-Krook models and the direct simulation Monte Carlo method for hypersonic flows, Phys. Fluids 30 (10) (2018) 106106.
[35] A.J. Lofthouse, Nonequilibrium Hypersonic Aerothermodynamics Using the Direct Simulation Monte Carlo and Navier–Stokes Models, PhD Thesis, University of Michigan, 2008.
[36] S. Chapman, T.G. Cowling, The Mathematical Theory of Non-Uniform Gases, Cambridge University Press, 1970.
[37] R.S. Myong, A full analytical solution for the force-driven compressible Poiseuille gas flow based on a nonlinear coupled constitutive relation, Phys. Fluids 23 (2011) 012002.
[38] M. Pfeiffer, Extending the particle ellipsoidal statistical Bhatnagar-Gross-Krook method to diatomic molecules including quantized vibrational energies, Phys. Fluids 30 (2018) 116103.
[39] F. Fei, Y. Hu, P. Jenny, A unified stochastic particle method based on the Bhatnagar-Gross-Krook model for polyatomic gases and its combination with DSMC, J. Comput. Phys. 471 (2022) 111640.